

# Non-planar Surface Shape Reconstruction from a Point Cloud in the Context of Muscles Attachments Estimation\*

Josef Kohout<sup>a</sup> and Martin Cervenka<sup>b</sup>

Faculty of Applied Sciences, University of West Bohemia, Technická 8, Plzeň, Czech Republic

**Keywords:** Shape Reconstruction, Point Cloud, Multidimensional Scaling, Muscle Attachments Estimation, Fast Marching, Scalar Distance Field.

**Abstract:** Knowledge of muscle attachments on bones is essential for musculoskeletal modelling. A muscle attachment is often represented by points (in 3D) obtained by a manual digitisation system during dissection. Although this representation suffices for many purposes, sophisticated musculoskeletal models commonly require representing a muscle attachment by a surface patch or at least by a closed boundary curve. In this paper, therefore, we propose an approach to automatic shape reconstruction from such point sets. It is based on iso-contour extraction from a scalar field of distances to geodetics connecting the pairs of points (from the input set) as identified by a state-of-the-art algorithm for 2D curve reconstruction running on the input points transformed to 2D. We investigated the performance of 15 existing state-of-the-art algorithms with public implementations on the TLEM 2.0 data set of muscle attachments. The best results were obtained for the lenz algorithm with just one unacceptable reconstruction when standard projection onto a best-fit plane was used to transform the input 3D points to 2D. The second algorithm was  $\alpha$ -shape with three unacceptable reconstructions, whereas in this case, the multidimensional scaling technique was exploited to transform the points.

## 1 INTRODUCTION

Shape reconstruction from a point cloud is an important computational geometry problem with various applications in computer graphics, computer vision, medical image analysis, pattern recognition, computer-aided design, cultural heritage, and others. During the past decades of research, many algorithms for shape reconstruction have been proposed. Some work with points sampled on the boundary of an object whose shape is to reconstruct, while others work with the points sampled in its interior. Some algorithms can deal (to some extent) with non-uniform or sparse sampling, noise or outliers, while others assume a dense uniform sampling. Some focus on specific kinds of objects, e.g., CAD objects with sharp edges or terrain data. Some require additional information, such as normals in points. However, most importantly, some work in 2D, processing 2D point

clouds to reconstruct the outlining contour of the object, while others work in 3D, processing 3D point clouds to reconstruct the outlining surface of the object. A good survey of algorithms of the former category can be found in (Ohrhallinger et al., 2021). For a survey of the algorithms of the latter category, we refer the reader to (Berger et al., 2016).

In this paper, we propose a novel algorithm for reconstructing a space curve from a set of 3D points. It employs the multidimensional scaling technique (Cox and Cox, 2008) to transform the points from 3D to 2D and then uses a suitable algorithm for 2D curve reconstruction to get the connectivity of the input points.

Motivation for our work lies in muscle attachment estimation. Knowledge of muscle attachments on bones is essential for musculoskeletal modelling. A muscle attachment is often represented by points obtained by a manual digitisation system during dissection. Due to the apparent effort associated with this process, no wonder that the sampling is sparse. Commonly, the points are unordered and exhibit a non-uniform distribution because it is natural to sample the upper side of the attachment area from left to right, then cut off the muscle-tendon unit and sample the lower side from left to right. The points are sub-

<sup>a</sup> <https://orcid.org/0000-0002-3231-2573>

<sup>b</sup> <https://orcid.org/0000-0001-9625-1872>

\*This Work Was Supported by the Meys of the Czech Republic, Project SGS-2019-016.

<sup>†</sup>Corresponding author

ject to various errors, introduced during the dissection (e.g., movements of the limbs, the ambiguity in defining the attachment boundary) or during the registration process. Sometimes a few points are even sampled in the interior of the attachment area. Figure 1 shows an example of such data.

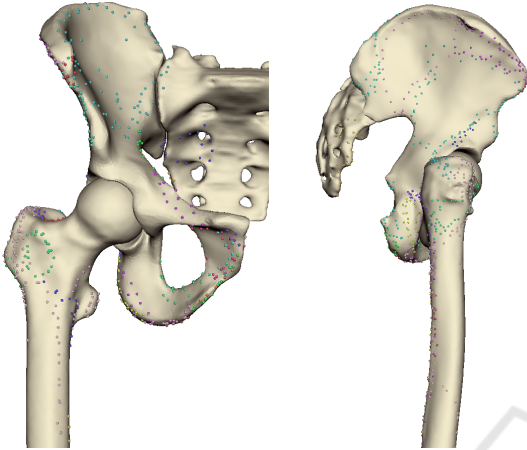


Figure 1: TLEM 2.0 (Carbone et al., 2015) data set containing point clouds defining various muscle attachments on lower limbs.

It can be seen that the attachment areas are only slightly curved. Therefore, a naive approach would be to project the points onto the best-fitted plane (obtained, e.g., by using the least-squares method) and then proceed with some of the existing state-of-the-art algorithms for reconstructing 2D curves. This paper investigates if exploiting the multidimensional scaling (MDS) technique would not improve the obtained results when comparing them with the ground truth. We experimented with 15 different algorithms.

Our other contribution is as follows. Since the 3D models of bones are available, we propose an approach to convert a non-manifold curve, which may result from the process, into a closed manifold one. It is based on iso-contour extraction from the scalar field on the surface of the bones that encodes distances to geodetics connecting the adjacent points of curves.

## 2 RELATED WORK

The problem of muscle attachments estimation was addressed in (Fukuda et al., 2017). The authors dissected individual muscles in the hip region of eight cadaver specimens while tracing the boundary of the muscle attachments using an optical tracker. The recorded points were manually refined to remove outlier measurements due to tracking noise. In this paper, we investigate if we could get the boundary of an at-

tachment automatically without the necessity of such manual refinement.

In their work, (Kohout and Kukačka, 2014) described a fully automatic algorithm for extraction of a closed region from a triangular model of a muscle, where region boundary is specified by a set of points lying on the muscle surface or in its vicinity. The points had to be specified in an order such that interconnecting every pair of adjacent points by a line segment would produce a closed non-intersecting polyline corresponding to the boundary of the region to extract. However, typical data sets of attachment areas do not comply with this requirement, as shown in Figure 1. In this paper, we investigate how to filter out the input points and order them to satisfy the requirement of this algorithm.

Approximating or interpolating the input points by an analytical function may be considered relevant to this problem. Most suitable seems to be radial basis function (RBF) approximation since the points are scattered and unordered. RBF was used for surface reconstruction of watertight 3D objects by (Carr et al., 2001). It is also commonly used for scattered data approximation in general (Cervenka et al., 2019). In this paper, we address the idea of transforming the input 3D points to 2D, finding the curve there (by exploiting RBF approximation) and returning to 3D space. One option for the points dimension reduction is the multidimensional scaling (MDS) technique (Cox and Cox, 2008), which is widely used in many different scientific fields.

Recently, (Ohrhallinger et al., 2021) designed a benchmark for a comprehensive quantitative evaluation of algorithms for 2D curves reconstruction. It consists of 14 curve reconstruction algorithms, including the recent ones, implemented in C++. Most of these algorithms construct a graph from the points and then filter the outline by some criteria. Most of them are parameterless, but only some are robust to noise and outliers.

## 3 OUR APPROACH

Given a set  $S = (P_i)$  of  $n$  points in 3D, sampled on a smooth curve on a non-planar smooth surface, including potentially noise or outliers, our task is to find an ordered set  $S' \subseteq S$  such that  $S'$  represents a closed non-intersecting space curve. The other points ( $S \setminus S'$ ) which do not lie on the curve are considered as outliers. Figure 2 shows an example of the input data.

Our basic idea is to exploit the multidimensional scaling (MDS) technique (Cox and Cox, 2008) to construct  $n$  points  $Q_i$  in 2D such that:

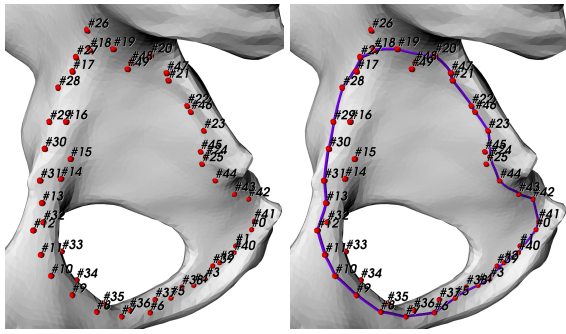


Figure 2: Obturator internus origin data set. Left - the input point set together with the order in which the points were sampled, right - the ground truth closed curve we specified manually according to anatomical atlases.

- every point  $Q_i$  is uniquely associated with just one point  $P_i$  so we are able to return back to 3D, and
- the distance between a pair of points  $Q_i, Q_j$  are as close to the distance between a pair of associated points  $P_i, P_j$  as possible.

Executing a 2D curve reconstruction algorithm on the set of points  $Q_i$  produces the sought connectivity between the points  $P_i$ . If the output connectivity forms a single closed curve, we are ready. Otherwise, the output must be filtered: some edges might need to be removed, some edges to close the curve might need to be inserted. We assume that the surface from which the data were sampled is available and is represented by a triangular model, or can be reconstructed from the input points, e.g., by using the RBF approach (see Section 3.1). It allows us to solve the filtering step in a rather unorthodox but straightforward approach.

Suppose the points  $P_i$  and  $P_j$  should be connected. At first, we subdivide the triangles of the surface mesh that contain these points in their vicinity, introducing thus these points as new vertices of the mesh. Then, we trace the shortest path connecting newly introduced vertices to a set of surface points  $P_{i,j,k}$ , as illustrated in Figure 3. The Dijkstra algorithm can be used for it, providing that the triangular model is fine enough. Some of the fast marching methods, see, e.g., (Peyré, 2009), is an alternative suitable in all cases.

We construct a scalar field  $SDF(V)$  on the surface of the mesh such that it returns the geodetic distance between the given surface point  $V$  and the nearest  $P_{i,j,k}$  point – see Figure 4. This field can be constructed easily using a bread-first search algorithm starting at  $P_{i,j,k}$  points. We adopt a fast marching method described in (Peyré, 2009) for this purpose.

An algorithm for iso-contours extraction is executed with the iso-value about the average length of edges  $P_{i,j,k}, P_{i,j,k+1}$ . In our experiments, we specify this value to  $0.5 \cdot (\min \|P_{i,j,k}, P_{i,j,k+1}\| + \max \|P_{i,j,k}, P_{i,j,k+1}\|)$ . Multiple contours are usually

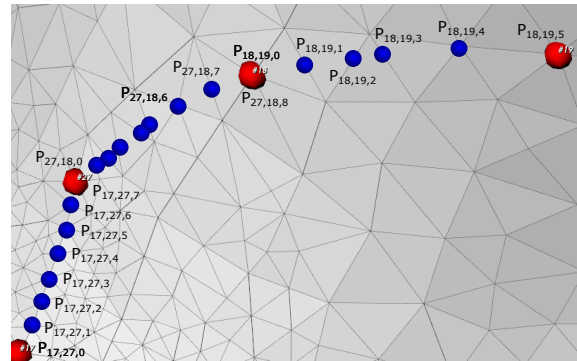


Figure 3: Refined edges  $P_{17}, P_{27}, P_{27}, P_{18}$ , and  $P_{18}, P_{19}$  of the obturator internus origin data set (see Figure 2) on the surface of the pelvis bone.

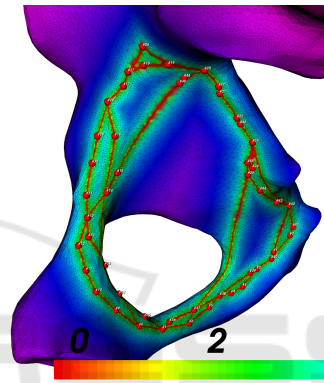


Figure 4: Scalar field constructed on the surface of the pelvis bone for the refined connectivity (obtained by (Lenz, 2006) algorithm) of the obturator internus origin data set.

extracted (e.g., one from the exterior of a closed curve, the other from the interior). The one with the largest perimeter is selected as a result – see Figure 5 for an example. We note that the final contour does not go through the input points but providing that the refinement of the primary edges is sufficient, this does not stand for a problem in many applications (including the muscle attachments estimation).

### 3.1 Radial Basis Functions (RBF)

Radial basis function interpolation and approximation is defined as follows:

$$h_i(x) = \sum_{j=1}^N \lambda_j \varphi(\|x_i - x_j\|), \quad (1)$$

$$\text{or also: } h = A\lambda, \quad A_{i,j} = \varphi(\|x_i - x_j\|)$$

The  $\lambda_i$  variable is the weight of a single RBF,  $\varphi$  denotes radial basis function,  $x_i$  and  $x_j$  are the positions of the input vertices (maybe attachment area vertices in our case), and  $h_i$  are values in the vertices.

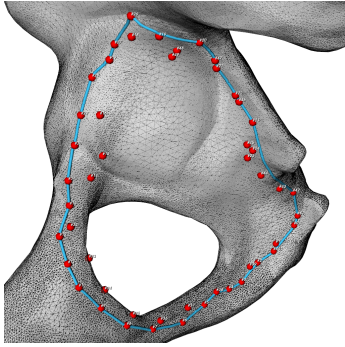


Figure 5: Obturator internus origin closed curve extracted from the scalar field in Figure 4. Compare it with the ground truth curve in Figure 2 right.

We experimented with a novel RBF described in (Skala and Cervenka, 2020) defined as:

$$\varphi(r) = r^2(r^a - 1) \quad (2)$$

Variable  $a$  is a shape parameter that has to be identified accurately to get good results. We also used  $a = 1.8$  as proposed by the original authors. Figure 6 shows the surface reconstructed by this approach from the input points. This surface can be used as an alternative to the triangulated model of a bone.

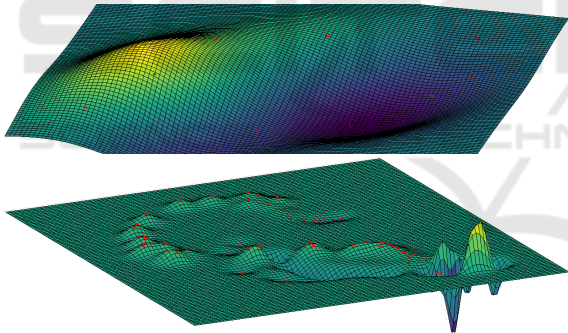


Figure 6: The surface of the femur bone reconstructed by the RBF method from the input points of biceps femoris origin (top) and vastus intermedius origin (bottom).

## 4 EXPERIMENTS AND RESULTS

The approach described above was implemented in C++ 14 using:

- the Visualization Toolkit (VTK)<sup>1</sup> for loading the data, curve reconstruction by the  $\alpha$ -shape algorithm (see (Edelsbrunner et al., 1983)), iso-lines extraction, and visualization of results,
- the benchmarking by (Ohrhallinger et al., 2021) for curve reconstruction by 14 different algo-

<sup>1</sup><https://vtk.org/>

rithms – connect2d, hnn crust, fitconnect, stretchdenoise, discour, vicur, crawl, peel, crust, nncrust, ccrust, gathan1, gathang, and lenz,

- the code by Yuki Koyama<sup>2</sup> for the multidimensional scaling,
- the geodesic computation on surfaces by (Krishnan, 2013), based on the fast marching method,
- and the Muscle Decomposition by (Kohout and Kukačka, 2014) for extracting the muscle attachment area bounded by the reconstructed curve from the surface mesh.

We note that the disk radius parameter of the  $\alpha$ -shape algorithm was set to 0.5625 times the maximal shortest distance between pairs of points, i.e., just enough to guarantee that the output will have one component only. The implementations of the other reconstruction algorithms were used with their default parameters.

We experimented with the point sets representing muscle attachments of a comprehensive TLEM 2.0 data set of lower limbs (Carbone et al., 2015). After performing initial analyses, we selected, more or less randomly, a couple of representative point sets for further experiments – see Figure 7. For each of the 27 point sets we ended with, we specified the ground-truth connection of the points according to depictions in anatomical atlases. We note that in some cases, the task of finding a proper connection has proven to be complicated even for a human expert.

We inserted the points into the surface mesh of the appropriate bone and used the geodesic computation to obtain the final closed ground-truth curve. An example of such a curve is in Figure 2, right.

Using the code for the muscle decomposition by (Kohout and Kukačka, 2014), we extracted the part of the mesh belonging to the attachment area bounded by the ground-truth closed curve. In three cases (adductor longus insertion, obturator internus origin and gluteus maximus inferior origin), the implementation failed to provide us with an acceptable result. This was caused by the fact that the input data violated the assumptions of the original method. Figure 8 shows examples of extracted ground-truth attachments.

We then ran our implementation. It provided us with 15 contours for each dataset, one for every curve reconstruction algorithm. For each output contour, the surface patch was extracted from the bone model in the same way as described above. Dice similarity coefficient (DSC) was computed to measure the dissimilarity between the outcome and the ground truth.  $DSC = 1$  means a perfect match, while  $DSC = 0$  means that the patches do not intersect. Naturally, the value of  $DSC$  depends on the sampling frequency.

<sup>2</sup><https://github.com/yuki-koyama/multidimensional-scaling/blob/master/mds.h>

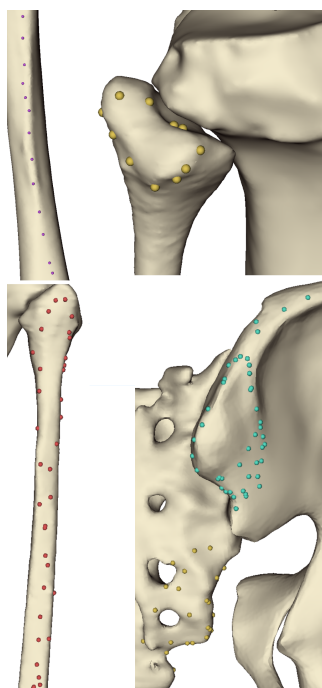


Figure 7: Representative examples of TLEM 2.0 point sets of muscle attachments. From top to bottom, left to right: biceps femoris origin, biceps femoris insertion, soleus lateralis origin, and gluteus maximus superior + inferior origin.

Our samples included all vertices of the bone mesh triangles plus some points sampled randomly in every triangle with an area larger than  $\epsilon$ . The number of samples in such a triangle was determined as its area divided by  $\epsilon$ . In the experiments, we used  $\epsilon = \pi \cdot 0.1 \cdot 0.1$ , which means our sampling frequency was about 0.2 mm.

Figure 9 shows the results we obtained. For closed curves with almost uniform sampling without apparent outliers and noise, represented, e.g., for biceps femoris insertion, the differences between 2D curve reconstruction algorithms are negligible. It is also apparent that only the  $\alpha$ -shape algorithm was robust enough to process every data set. Connect2d, fitconnect, discurs, and vicur algorithms could process only about 70.8% of data sets, stretchdenoise only about 58.3%. The rest failed to process the gluteus medius posterior insertion, which is not surprising considering that this data set contains many outliers (see Figure 10). The poor performance, generally, showed discurs and vicur algorithms.

Further inspection reveals that none of the algorithms could provide acceptable results for the gluteus maximus inferior insertion and vastus intermedius origin data sets. In the former case, the reason is simply that the data contains three outliers outside the attachment region (probably introduced during an er-

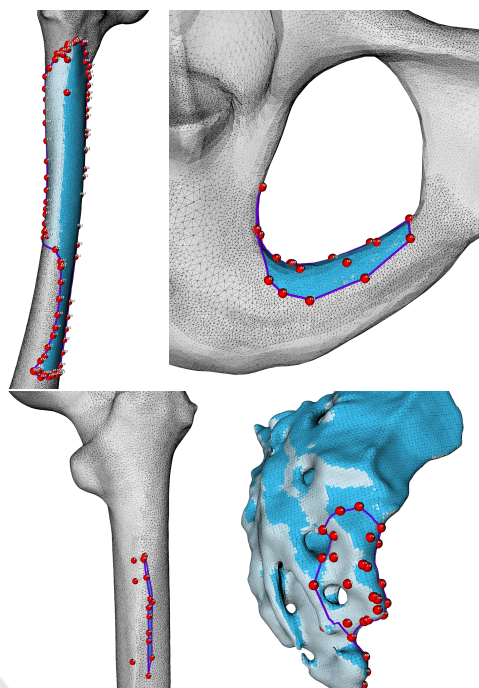


Figure 8: Ground-truth closed curves (purple) for vastus intermedius origin, obturator externus lateral origin, gluteus maximus inferior origin, and gluteus maximus inferior insertion. Surface patches representing the attachment areas, extracted using the implementation by (Kohout and Kukačka, 2014) are shaded in blue.

roneous registration process) – see Figure 10. In the latter case, the explanation is more complicated. Although the data of vastus intermedius origin seems quite OK for a human observer (see Figure 8), the algorithms yield multiple connections between the points on the left side with those on the right one. It might be because the sampling frequency on the boundary is insufficient, and thus the influence of the single apparent outlier is not negligible. As the femur bone resembles a cylinder, the geodetics computed for these incorrect edges are not on the same side, but some lie in the front, others in the back. As a result, the bone is effectively cut into several parts, as shown in Figure 10 and, therefore, only a part of the attachment area is extracted.

On average, the best performance reached  $\alpha$ -shape (72.00%), followed by connect2d (69.35%), and lenz (67.04%). However, it is needed to point out that the dice similarity coefficient is not a reliable indicator for very narrow attachments represented by slightly curved lines, for which values as low as 30% are often visually acceptable. This is the case of adductor longus insertion, adductor magnus mid insertion, adductor magnus proximal insertion, biceps femoris CB origin, iliopsoas superior in-

| Muscle attachment                  | alpha shape   | connect2d     | hncrust | fitconnect    | stretchdenoise | discur | vicur  | crawl         | peel          | crust  | nncrust       | ccrust        | gathan1       | gathang       | lenz          |
|------------------------------------|---------------|---------------|---------|---------------|----------------|--------|--------|---------------|---------------|--------|---------------|---------------|---------------|---------------|---------------|
| adductor magnus distal insertion   | <b>94.64%</b> | 87.58%        | 28.79%  | 92.49%        | 92.49%         | 0.48%  | 14.31% | 34.14%        | 28.37%        | 24.80% | <b>93.70%</b> | 14.57%        | 26.01%        | 26.01%        | 93.38%        |
| adductor magnus mid insertion      | <b>78.88%</b> | 51.98%        | 28.83%  | 28.83%        |                | 28.83% | 28.83% | 28.83%        | 25.86%        | 28.83% | 28.83%        | 52.22%        | 28.83%        | 72.11%        |               |
| adductor magnus proximal insertion | 85.06%        | <b>81.97%</b> | 24.83%  | 24.83%        | 24.83%         | 24.83% | 24.83% | 22.88%        | 24.72%        | 21.36% | 21.36%        | 21.36%        | <b>81.83%</b> | 21.36%        | <b>86.38%</b> |
| biceps femoris origin              | <b>84.72%</b> | 54.63%        | 19.09%  | 19.09%        | 19.09%         | 19.09% | 19.09% | 20.48%        | 19.58%        | 20.48% | 20.48%        | 20.48%        | 54.84%        | 20.48%        | 26.02%        |
| biceps femoris insertion           | <b>98.44%</b> | 97.23%        | 97.23%  | 97.23%        | 97.23%         | 97.23% | 97.23% | 97.23%        | 97.23%        | 97.23% | 97.23%        | 97.23%        | 97.23%        | 97.23%        | 97.95%        |
| gluteus maximus inferior insertion | 16.46%        |               | 31.96%  |               |                |        |        | 28.91%        | 28.68%        | 30.09% | 27.92%        | 27.92%        | 31.64%        | <b>35.42%</b> | 17.31%        |
| gluteus maximus superior insertion | <b>89.67%</b> |               | 21.92%  |               |                |        |        | 33.59%        | 25.10%        | 29.46% | <b>91.06%</b> | 14.44%        | 15.27%        | 18.40%        | 83.66%        |
| gluteus maximus superior origin    | 79.92%        | 87.56%        | 5.78%   | 76.52%        | 76.52%         | 3.88%  | 3.55%  | <b>94.14%</b> | 8.10%         | 6.89%  | <b>81.34%</b> | 3.19%         | 4.26%         | 7.18%         | 77.98%        |
| gluteus medius anterior insertion  | <b>91.48%</b> | 83.15%        | 7.05%   | 89.35%        | 89.35%         | 16.23% | 11.39% | 20.65%        | 12.97%        | 10.01% | 65.61%        | 14.41%        | 8.62%         | 15.88%        | 84.84%        |
| gluteus medius anterior origin     | 96.84%        |               | 7.22%   |               |                |        |        | 13.09%        | 10.72%        | 5.59%  | <b>93.02%</b> | 2.91%         | 4.24%         | 5.21%         | <b>97.47%</b> |
| gluteus medius posterior insertion | <b>79.40%</b> |               |         |               |                |        |        |               |               |        |               |               |               |               |               |
| gluteus medius posterior origin    | 97.31%        | 98.11%        | 98.11%  | 97.98%        | 97.98%         | 3.73%  | 98.08% | 98.11%        | 98.11%        | 98.11% | 98.11%        | 4.00%         | 98.11%        | 98.11%        | <b>98.36%</b> |
| iliopsoas inferior insertion       | <b>96.17%</b> | 77.17%        | 8.82%   | 54.97%        | 54.97%         | 0.91%  | 16.68% | 25.79%        | 17.46%        | 18.71% | 47.84%        | 11.75%        | 9.54%         | 17.81%        | 95.59%        |
| iliopsoas superior insertion       | <b>71.98%</b> | 65.20%        | 49.47%  | 49.47%        | 49.47%         | 49.47% | 49.47% | 32.39%        | 32.39%        | 49.47% | 49.47%        | 49.47%        | 49.47%        | 49.47%        | 66.23%        |
| obturator externus lateral origin  | <b>89.09%</b> | 62.48%        | 9.62%   | <b>11.78%</b> |                | 5.23%  | 12.28% | 17.84%        | 10.30%        | 17.15% | 65.52%        | 7.38%         | 45.24%        | 6.08%         | 78.82%        |
| obturator externus medial origin   | <b>97.89%</b> | 78.36%        | 6.40%   | <b>80.84%</b> | <b>80.84%</b>  | 6.48%  | 4.82%  | 10.11%        | 6.14%         | 6.62%  | 89.87%        | 5.68%         | 1.50%         | 7.51%         | 96.77%        |
| sartorius insertion                | 48.95%        |               | 20.88%  |               |                |        |        | 61.61%        | 34.42%        | 35.86% | <b>74.81%</b> | 40.69%        | 35.02%        | 48.11%        | 59.02%        |
| semimembranosus insertion          | <b>78.91%</b> | 72.93%        | 34.34%  | 34.34%        | 34.34%         | 34.34% | 34.34% | 24.14%        | 34.85%        | 24.14% | 24.14%        | 24.14%        | 72.80%        | 24.14%        | 78.88%        |
| semimembranosus origin             | 70.16%        | <b>87.90%</b> | 12.20%  | 8.95%         | 8.95%          | 1.89%  | 9.28%  | 19.69%        | 12.62%        | 23.40% | 56.29%        | 8.91%         | 13.53%        | 79.03%        | 73.13%        |
| soleus lateralis origin            | <b>71.05%</b> | 45.73%        | 15.31%  | 15.52%        | 15.52%         | 3.64%  | 7.07%  | 15.55%        | 14.89%        | 11.36% | 15.56%        | 10.60%        | 51.43%        | 11.66%        | 16.24%        |
| soleus medialis origin             | <b>15.38%</b> | 12.28%        | 48.25%  | 46.16%        | 46.16%         | 15.54% | 47.63% | 48.43%        | 44.07%        | 45.44% | 19.33%        | <b>51.41%</b> | 12.27%        | 12.27%        | 14.24%        |
| vastus intermedius origin          | 0.06%         |               | 6.73%   |               |                |        |        | 11.19%        | 6.42%         | 10.56% | 36.09%        | 4.49%         | 22.82%        | 4.00%         | <b>39.64%</b> |
| vastus medialis inferior origin    | 36.76%        |               | 31.47%  |               |                |        |        | 41.63%        | <b>42.55%</b> | 40.60% | 41.45%        | 41.45%        | 38.42%        | 41.45%        | 33.87%        |
| vastus medialis superior origin    | <b>58.85%</b> | 34.74%        | 14.56%  | 25.18%        |                | 20.83% | 8.65%  | 23.99%        | 13.34%        | 13.32% | 44.78%        | 12.14%        | 13.00%        | 15.50%        | 53.97%        |

Figure 9: Dice similarity coefficients of various muscle attachments, obtained for the MDS with different curve reconstruction algorithms. Missing values mean that the reconstruction algorithm failed. The best performances are marked in bold.

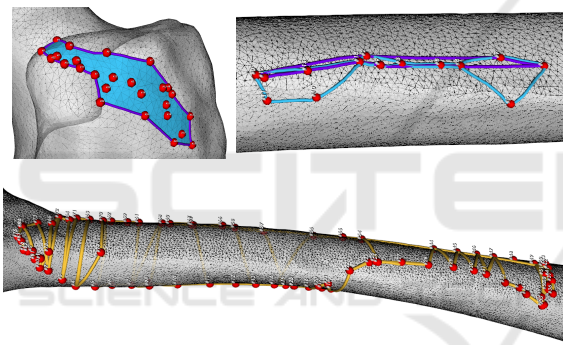


Figure 10: The data sets causing troubles during the processing (see the text): gluteus medius posterior insertion with a lot of internal points (top left), gluteus maximus inferior insertion with three outer points (top right), and vastus intermedius origin with an insufficient sampling frequency (bottom). The ground-truth curve is purple, the final contour obtained from  $\alpha$ -shape curve is light blue, and geodetics computed from the connectivity found by the lenz algorithm are yellow.

sertion, semimembranosus insertion, soleus medialis origin, and vastus medialis inferior origin. If we exclude the results of these data sets, we get four algorithms whose performance exceeds 70% on average:  $\alpha$ -shape (78.74%), lenz (76.45%), connect2d (76.36%), and nncrust (70.05%). Considering that connect2d failed repeatedly, we can recommend only  $\alpha$ -shape or lenz algorithms for the curve reconstruction in our context.

For the data sets mentioned above, a better indicator might be the difference in the perimeter of the reconstructed and ground-truth curves. Table 1 shows that according to this indicator, the best performing

algorithm is connect2d, with the error of 1.25% on average but one failure, followed by gathan1 (2.60% on average),  $\alpha$ -shape (3.03%), and lenz (3.43%). All other algorithms exhibited a worse performance with multiple failures or average errors exceeding 4% (in absolute values). We note that median errors were below 4% in all cases. The order of the five best-performing algorithms remains the same even when median errors are considered.

Therefore, it can be concluded that  $\alpha$ -shape or lenz algorithms are universal algorithms suitable for all cases. This result is also confirmed by a subjective test, in which a human volunteer assessed all the reconstructed contours visually, classifying them into three categories:

- A = no issue or a minor one only without any considerable impact on musculoskeletal modelling,
- B = acceptable but with some issues that might have some undesirable impacts on musculoskeletal modelling, and
- C = unacceptable.

The  $\alpha$ -shape and lenz algorithms have almost half of their contours (48.1% precisely in both cases) in category A. While hncrust, discur, vicur, peel, crust, ccrust, gathan1, and gathang algorithms have more than half of the contours they produced in category C,  $\alpha$ -shape and lenz have there only 4 and 5 contours, which corresponds to 11.1% and 18.5%, respectively. Two of these contours belong to gluteus maximus inferior insertion, and vastus intermedius origin, already discussed above (see also Figure 10).  $\alpha$ -shape further failed to provide acceptable results for vastus medialis superior origin, lenz for obturator externus

Table 1: Differences between the perimeters of the reconstructed and ground-truth contours for selected 2D curve reconstruction algorithms. The best results are bold.

| Name                               | $\alpha$ -shape | connect2d     | fitconnect   | nncrust       | gathan1       | lenz         |
|------------------------------------|-----------------|---------------|--------------|---------------|---------------|--------------|
| adductor longus insertion          | 7.73%           | <b>5.82%</b>  | 7.85%        | 7.84%         | <b>5.82%</b>  | 8.26%        |
| adductor magnus mid insertion      | 1.54%           | <b>0.00%</b>  | 1.07%        | 1.07%         | <b>0.00%</b>  | 0.92%        |
| adductor magnus proximal insertion | 2.31%           | <b>-0.20%</b> | 3.79%        | 3.71%         | <b>-0.20%</b> | 3.11%        |
| biceps femoris origin              | 1.25%           | <b>-0.28%</b> | 1.37%        | 0.73%         | <b>-0.28%</b> | 1.41%        |
| iliopsoas superior insertion       | 6.69%           | <b>0.70%</b>  | 8.35%        | 8.35%         | 8.35%         | 7.05%        |
| semimembranosus insertion          | 1.85%           | <b>-0.04%</b> | 2.48%        | 2.68%         | <b>-0.04%</b> | 1.97%        |
| soleus medialis origin             | -1.31%          | -2.98%        | -5.75%       | <b>-0.22%</b> | -2.99%        | -0.84%       |
| vastus medialis inferior origo     | <b>1.59%</b>    |               |              | 7.63%         | 3.09%         | 3.86%        |
| <b>Avg(abs(error))</b>             | <b>3.03%</b>    | <b>1.25%</b>  | <b>3.83%</b> | <b>4.03%</b>  | <b>2.60%</b>  | <b>3.43%</b> |

lateral origin, soleus lateralis origin, and soleus medialis origin. In all four cases, the attachments are much more stretched in one dimension than in the other. Due to sparse sampling, the MDS increased further this ratio, producing points visually lying almost on a one-dimensional object (see Figure 11). All algorithms then struggled with such data.

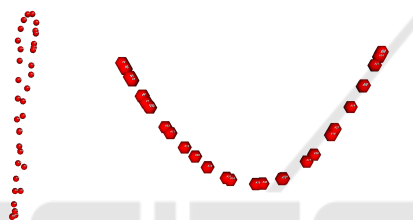


Figure 11: Soleus lateralis origin after being transformed into 2D using projection onto the best fit plane (left) and using the multidimensional scaling technique (right).

We, therefore, compared the results with those obtained when the input points were projected onto the plane fitted to the data by the least-squares method instead of using the multidimensional scaling technique. Table 2 show that although some algorithms benefit from the MDS technique (e.g., fitconnect, stretchdenoise, or peel), others, without any doubt, perform better without it (e.g., lenz or nncrust). As for the subjective tests, lenz algorithm came in first with 15 (i.e., 55.6%) muscle attachments in category A, 11 (i.e., 40.7%) in category B and only vastus intermedius origin in category C. The second place was taken by  $\alpha$ -shape with 10 (i.e., 37%) muscle attachments in category A, 13 (i.e., 48.1%) in category B, and 4 (i.e., 14.8%) in category C. Clearly, while  $\alpha$ -shape achieved more acceptable results with the MDS, lenz demonstrated different behaviour.

However, we must point out that a projection of points onto a common plane is not suitable when the curve to be reconstructed bends several times, e.g., like in the case of a narrow saddle. Although such cases are pretty rare in the context of muscle attachments, they seem to be frequent in the aneurysm neck identification problem.

Table 2: Difference of the average performance when using the MDS and when using the projection onto a common plane. Positive values mean that the MDS outperforms the projection. Dice similarity coefficients (DSC) are used as a performance indicator for the data for which DSC is a reliable indicator (see the text for explanation). For the rest, errors in the muscle attachments perimeters (PER) are used.

| Algorithm       | DSC     | PER     |
|-----------------|---------|---------|
| $\alpha$ -shape | -0.37%  | -0.31%  |
| connect2d       | -8.80%  | 0.23%   |
| hnnncrust       | 8.83%   | 0.00%   |
| fitconnect      | 11.54%  | 0.25%   |
| stretchdenoise  | 17.10%  | -0.26%  |
| discur          | -8.46%  | 6.38%   |
| vicur           | -5.70%  | -0.01%  |
| crawl           | -6.69%  | -0.03%  |
| peel            | 9.61%   | 0.05%   |
| crust           | 4.31%   | -0.08%  |
| nncrust         | -6.63%  | -0.57%  |
| ccrust          | -0.17%  | -6.31%  |
| gathan1         | 3.87%   | -2.11%  |
| gathang         | -12.59% | -11.09% |
| lenz            | -12.66% | -0.72%  |

We also did some preliminary testing of the RBF approach for ordering the vertices and smoothing the curve. The primary purpose of this test is to check whether the RBF approach will be capable of creating a closed and non-self-intersecting curve in 2D.

If the outliers or apparent nonuniformity are present, the resulting curve is far from expectations (e.g. vastus intermedius origin on the left of Figure 12). Luckily, this approach gives better results for many other attachment areas (e.g. gluteus medius posterior on the right of the Figure 12). The polar coordinate system for the dimension reduction causes problems in some cases, mainly if there is a wide angle without any vertex (left image of the Figure 12, bottom part), causing a single or even multiple self-intersectional loops. Approximating the curve instead of interpolating may solve these issues.

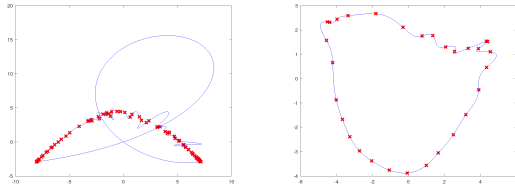


Figure 12: Two radial basis function approximation results. Vastus intermedius origin is on the left. The connection between both ends of the attachment area does not turned out well due to looping the curve. Gluteus medius posterior origin is on the right. The shape is approximated by expectations.

## 5 CONCLUSION AND FUTURE WORK

This paper investigated the options of reconstructing a closed space curve from the points sampled on that curve, supporting sparse sampling and noisy data with multiple outliers. Our extensive experiments, performed on the TLEM 2.0 data sets (Carbone et al., 2015) in the context of muscle attachments estimation, lead us to the following recommendations. If the curve to be reconstructed is not expected to have a shape of a narrow saddle or be otherwise strangely bent, the points should be projected onto the plane that best fit the input data. The lenz algorithm (Lenz, 2006) should be used on the projected points to find the primary connectivity between the input points. Suppose this algorithm is unavailable or the expectations on the curve shape do not hold. In that case, the input data should be transformed onto the plane using the multidimensional scaling (MDS) technique (Cox and Cox, 2008). The  $\alpha$ -shape algorithm (Edelsbrunner et al., 1983) should be then used on the transformed points (instead of the lenz algorithm), with the disc radius being slightly above half of the maximal shortest distance between pairs of transformed points. If neither algorithm is available, connect2d or nncrust (see (Ohrhallinger et al., 2021)) are a decent choice.

Providing that the surface on which the space curve lies is available, the reconstructed curve can be refined by tracing the shortest paths between each pair of points connected by an edge. A non-manifold curve, i.e., a curve containing vertices of valence larger than 2, can be converted into a manifold one using the algorithm proposed in the paper, based on iso-contour extraction from a scalar field describing for each point on the surface its distance to the curve. If the object bounded by the curve covers only a tiny portion of the surface in any direction or the surface is open, this conversion is reliable.

## REFERENCES

- Berger, M., Tagliasacchi, A., Seversky, L. M., Alliez, P., Guennebaud, G., Levine, J. A., Sharf, A., and Silva, C. T. (2016). A survey of surface reconstruction from point clouds. *Computer Graphics Forum*, 36(1):301–329.
- Carbone, V., Fluit, R., Pellikaan, P., van der Krogt, M., Janssen, D., Damsgaard, M., Vigneron, L., Feilkas, T., Koopman, H., and Verdonshot, N. (2015). TLEM 2.0 – a comprehensive musculoskeletal geometry dataset for subject-specific modeling of lower extremity. *Journal of Biomechanics*, 48(5):734–741.
- Carr, J. C., Beatson, R. K., Cherrie, J. B., Mitchell, T. J., Fright, W. R., McCallum, B. C., and Evans, T. R. (2001). Reconstruction and representation of 3d objects with radial basis functions. In *Proceedings of the 28th annual conference on Computer graphics and interactive techniques*. ACM Press.
- Cervenka, M., Smolik, M., and Skala, V. (2019). A new strategy for scattered data approximation using radial basis functions respecting points of inflection. *Computational Science and Its Applications*.
- Cox, M. A. A. and Cox, T. F. (2008). Multidimensional scaling. In *Handbook of Data Visualization*, pages 315–347. Springer Berlin Heidelberg.
- Edelsbrunner, H., Kirkpatrick, D., and Seidel, R. (1983). On the shape of a set of points in the plane. *Information Theory, IEEE Transactions on*, 29:551 – 559.
- Fukuda, N., Otake, Y., Takao, M., Yokota, F., Ogawa, T., Uemura, K., Nakaya, R., Tamura, K., Grupp, R. B., Farvardin, A., Armand, M., Sugano, N., and Sato, Y. (2017). Estimation of attachment regions of hip muscles in CT image using muscle attachment probabilistic atlas constructed from measurements in eight cadavers. *Int J Comput Assist Radiol Surg.*, 12(5):733–742.
- Kohout, J. and Kukačka, M. (2014). Real-time modelling of fibrous muscle. *Computer Graphics Forum*, 33(8):1–15.
- Krishnan, K. (2013). Geodesic computations on surfaces. *The VTK Journal*.
- Lenz, T. (2006). How to sample and reconstruct curves with unusual features. In *Proceedings of the 22nd European Workshop on Computational Geometry (EWCG)*, pages 29–32.
- Ohrhallinger, S., Peethambaran, J., Parakkat, A. D., Dey, T. K., and Muthuganapathy, R. (2021). 2d points curve reconstruction survey and benchmark. *Computer Graphics Forum*, 40(2):611–632.
- Peyré, G. (2009). Geodesic methods in computer vision and graphics. *Foundations and Trends® in Computer Graphics and Vision*, 5(3-4):197–397.
- Skala, V. and Cervenka, M. (2020). Novel rbf approximation method based on geometrical properties for signal processing with a new rbf function: Experimental comparison. *2019 IEEE 15th International Scientific Conference on Informatics*.